Pushing the limits of sensitivity and resolution for natural abundance ^{43}Ca NMR using ultra-high magnetic field (35.2 T)

Christian Bonhomme,*[a] Xiaoling Wang,[b] Ivan Hung,[b] Zhehong Gan,[b] Christel Gervais,[a] Capucine Sassoye,[a] Jessica Rimsza,[c] Jingcheng Du,[c] Mark E. Smith,[d] John V. Hanna,[e] Stéphanie Sarda,[f] Pierre Gras,[g] Christèle Combes,[g] and Danielle Laurencin*[h]

[a.] *Sorbonne Universités, CNRS, Collège de France, Laboratoire de Chimie de la Matière Condensée de Paris, LCMCP, F-75005 Paris, France (CB: christian.bonhomme@upmc.fr)*
[b.] *National High Magnetic Field Laboratory, 1800 East Paul Dirac Drive, Tallahassee, FL 32310–3706, USA.*
[c.] *Department of Materials Science and Engineering, University of North Texas, Denton, Texas 76207, USA*
[d.] *Department of Chemistry, Lancaster University, Lancaster LA1 4YB, UK*
[e.] *Department of Physics, Warwick University, Coventry, CV4 7AL, UK*
[f.] *CIRIMAT, Université de Toulouse, CNRS, Université Paul Sabatier,4 allée E. Monso, 31030 Toulouse cedex 4, France*
[g.] *CIRIMAT, Université de Toulouse, CNRS, INPT - Ensiacet, 4 allée E. Monso, 31030 Toulouse cedex 4, France*
[h.] *ICGM, UMR 5253, CNRS-UM-ENSCM, Place E. Bataillon, CC1701, 34095 Montpellier cedex 05, France (DL : danielle.laurencin@umontpellier.fr)*

Supporting Information

Synthetic procedures

The crystalline Ca-pyrophosphate phases, namely monoclinic calcium pyrophosphate tetrahydrate in the β phase (m-CPPT β, *m*-$Ca_2P_2O_7.4H_2O$), and triclinic calcium pyrophosphate dihydrate (t-CPPD, *t*-$Ca_2P_2O_7.2H_2O$), as well as the related amorphous compound referred to as a-CPP (composition $Ca_2P_2O_7.xH_2O$, with x ~ 4), were prepared as described in the literature.[1]

The crystalline Ca-oxalate monohydrate phase ($CaC_2O_4.H_2O$, COM) was synthesized according to a previously published procedure.[2]

The ^{43}Ca-labeled Ca-monetite phase was synthesized using $CaCO_3$ (partially enriched in ^{43}Ca) and H_3PO_4 as precursors. First, a mixture of 41 mg of ^{43}Ca-labeled $CaCO_3$ (60%-labelling, CortecNet) and 85 mg of non-labeled $CaCO_3$ (Aldrich) was heated to 1000°C under a flow of Ar.
After cooling to room temperature, ~70 mg of ^{43}Ca-enriched CaO were recovered (^{43}Ca-enrichment level ~20%). The labeled *CaO powder (~ 70 mg; n(Ca) ~ 1.25 mmol) was then transferred into a centrifuge tube, in which 1.5 mL of HPLC-grade water were added. The suspension was heated to 90°C under stirring (in an Ar atmosphere), before adding drop by drop 1.37 mL of a 1.00 mol.L^{-1} aqueous solution of H_3PO_4 (n(P) ~ 1.37 mmol). An additional 0.5 mL of HPLC-grade water was added to the medium, which was heated to 90°C for 3 days. Given that the goal of this synthesis was initially to prepare hydroxyapatite ($Ca_{10}(PO_4)_6(OH)_2$, Ca/P = 1.67), but that the "P" content initially added was too high, an additional amount of non-labelled Ca was then added after 3 days (in the form of an aqueous suspension of Ca-(hydr)oxide), in order to increase the Ca/P ratio in the reaction medium. Moreover, an additional amount of base (added under the form of an aqueous solution of NH_4OH) was then added. After 3 more days of stirring, the suspension was centrifuged, thoroughly washed several times with HPLC water, and then dried for 10 h at 100°C under vacuum. A total amount of 220 mg of precipitate was isolated.
The compound was then characterized by powder X-ray diffraction (Figure S1), showing that it mainly contains 2 crystalline phases ($CaHPO_4$ and $Ca(OH)_2$), and a small amount of hydroxyapatite. ^{43}Ca NMR analyses were then carried out, revealing that the ^{43}Ca NMR spectrum is similar to the previously reported data of $CaHPO_4$ (Figure S2).[3] The resonance of $Ca(OH)_2$ (δ_{iso} ~ 71 ppm; C_Q ~ 2.6 MHz) is not observed, meaning that this impurity is not significantly labeled (and hence not visible in ^{43}Ca NMR).

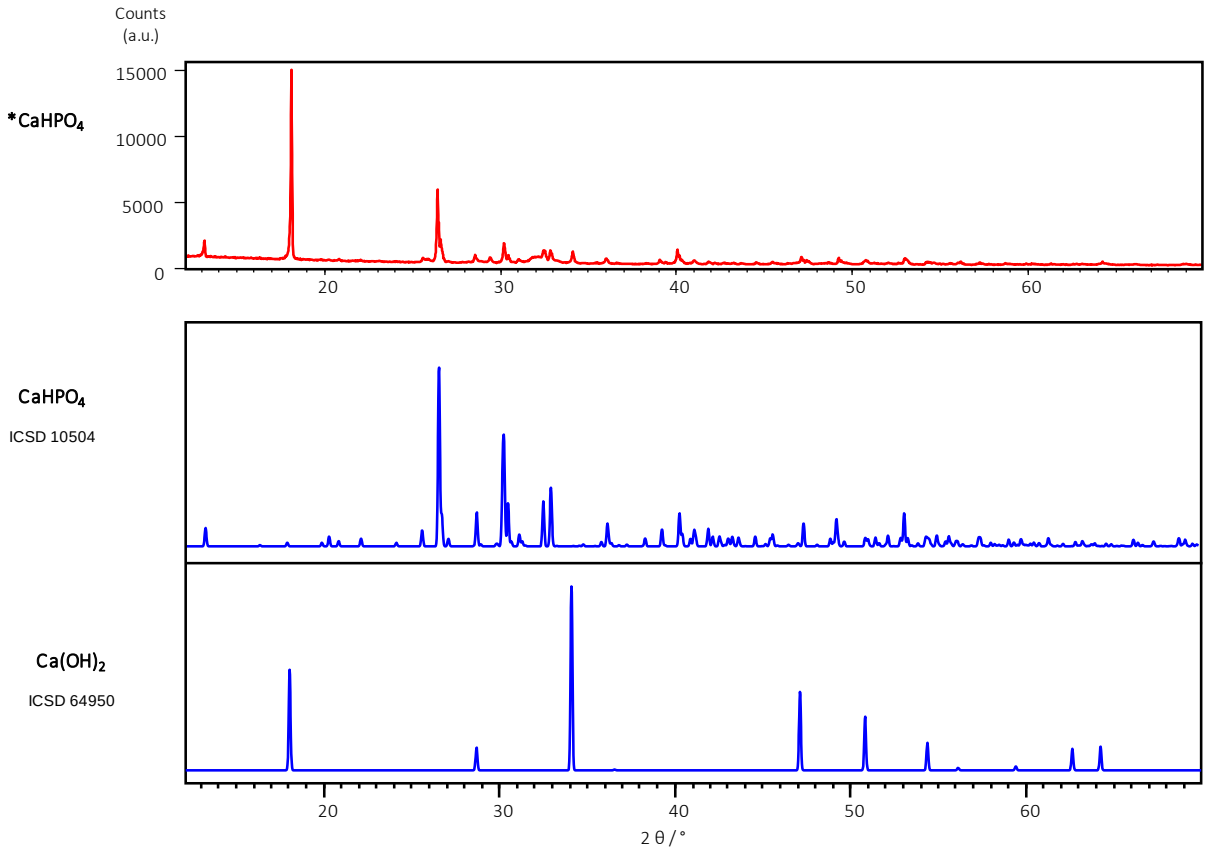

Figure S1. Experimental XRD powder pattern of the ^{43}Ca-enriched phase (top in red, *$CaHPO_4$), in comparison to published patterns for $CaHPO_4$ and $Ca(OH)_2$.

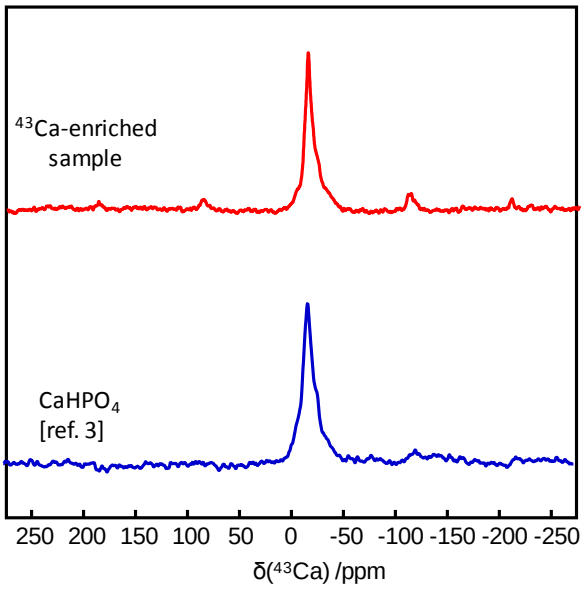

Figure S2. ^{43}Ca MAS NMR spectrum recorded at 14.1 T for the labeled phase (top), in comparison with the previously reported NMR spectrum of $CaHPO_4$ recorded at the same field at natural abundance (bottom).[3]

NMR acquisition parameters at 35.2 T

All experiments were carried out at 35.2 T, using a single-channel 3.2 mm MAS probe, tuned to ^{43}Ca ($\nu_0(^{43}Ca)$ = 100.96 MHz). Experiments were performed under temperature regulation (T = 283 K). Out of the five samples analyzed, only *$CaHPO_4$ was labeled in ^{43}Ca. Spectra were referenced to a 1.00 mol.L^{-1} solution of $CaCl_2$.

Table S1. Summary of the NMR acquisition parameters.

Sample	NMR sequence	Relaxation delay (s)	NS	total exp. time	ν_r (kHz)
*$CaHPO_4$	multi-dfs [(a)]	0.5	1k	3 min	10
*$CaHPO_4$	3Q echo shifted MQMAS [(b)]	0.5	96 *per* incr.	52 min	10
t-CPPD	multi-dfs[(a)]	0.5	114k	3 hours	18
m-CPPT β	wurst zg[(c)]	0.8	11k	2.5 hours	10
COM	zg	0.8	13k	3 hours	10
a-CPP	multi-dfs[(a)]	0.2	268k	3 hours	10

[(a)]4 blocks of DFS (optimized)[4], DFS pulse length: 5 ms (optimized), followed by a 90° selective pulse: 10 µs (at power level: 10 W – which corresponds to 6.25 kHz based on measurements on a solution of $CaCl_2$).
[(b)]excitation pulse: 3 µs – reconversion pulse: 1µs at power level: 400 W (39.5 kHz), echo delay: 982 µs (optimized), SPAM:[5] 90°: 6 µs at power level: 20W (8.8 kHz), 64 t_1 increments.
[(c)] WURST pulse[6]: 5 ms at power level: 13W (7.1 kHz).

It is worth mentioning that our attempts to record the *natural abundance* ^{43}Ca MAS NMR spectrum of a *highly crystalline* hydroxyapatite ($Ca_{10}(PO_4)_6(OH)_2$) were unsuccessful at this stage (despite the high $\%_{wt}$(Ca)). The hydroxyapatite sample analysed here was purchased from Biorad, and showed a very high crystallinity in X-Ray diffraction. This specific sample had not been studied by ^{43}Ca NMR at other fields before.
The main cause of this failure is most probably the long relaxation delay (due to the high crystallinity of the sample), as has been also noticed in the past for other Ca-compounds. Hence, the effect of relaxation has to be taken into account by users, as « overnight experiments » are not feasible currently at the ultra-high magnetic field facility.

Previously reported ^{43}Ca NMR parameters for the m-CPPT β, t-CPPD and COM crystalline phases

Table S2. Experimental *vs* calculated ^{43}Ca NMR parameters.

	Site	δ_{iso} (ppm)		C_Q (MHz)		η_Q	
		Exp	Calc	Exp	Calc	Exp	Calc
t-CPPD[7]	Ca1	14.5	13.8	3.4	−3.11	0.3	0.42
	Ca2	12.0	12.0	2.7	−2.47	0.5	0.14
m-CPPT β[7]	Ca1	11.0	11.9	1.8	1.57	0.6	0.43
	Ca2	7.5	11.4	2.1	2.36	0.6	0.67
COM[2]	Ca1	-2.6	-1.7	1.5	-1.34	0.6	0.99
	Ca2	0.7	4.2	1.6	1.68	0.7	0.59

Computational modeling: generation of models of the amorphous phase (a-CPP) by Ab Initio Molecular Dynamics (AIMD)

The development of amorphous calcium pyrophosphate (a-CPP) models is based on a multi-step protocol to ensure the development of isolated pyrophosphate anions (rather than phosphate chains or isolated orthophosphate ions), to which cations and water molecules are then added to generate an inverted glass structure. Initial placement of phosphorous atoms utilized a stochastic Monte Carlo (MC) process, as implemented in the RMCA code.[8]

Using an initial random mixture of 12 P atoms, MC was used to ensure a separation distance of 2.9-3.3 Å between the phosphate atoms. This is consistent with a P-P interatomic distance of ~ 2.9-3.0 Å, as reported in experimental pyrophosphate systems. Once this criterion had been satisfied, bridging oxygen atoms were placed between pairs of phosphorous atoms and radial oxygen were placed around the phosphate atoms to form a coordination number of four and generate the pyrophosphate species. The relaxation of the system was performed using periodic DFT calculations, starting with relaxation of the pyrophosphate systems alone (i.e. without including cations or water molecules). In this case, the charge of the systems due to the $P_2O_7^{4-}$ molecules was offset by the application of a background charge. The systems were relaxed to an energy minimum (~ 250 steps) and then systems were hydrated with water, and calcium cations were added at the appropriate ratio (Ca/P = 1). To confirm the density of the systems a cell optimization was performed to ensure the generation of systems at thermo-mechanical equilibrium at zero atmospheric pressure. This consisted of cell size optimization through which the cell dimensions were adjusted to identify the ideal density. A geometry optimization was performed between each cell optimization step to maintain the correct a-CPP structure. After the cell size optimization, *ab initio* molecular dynamics (AIMD) simulations for 5 ps (1 fs time step) were performed under the NVT ensemble at 300 K using a Nose-Hoover thermostat to further relax the generated structure models. A final geometry optimization step was performed following *AIMD* with an energy convergence of 1.0E-4 and a force convergence of 1.0E-3. Following the structural relaxation, a higher self-consistency accuracy (1E-10) relaxation before the GIPAW calculation was performed (discussed below).

Pair Distribution Function (PDF) analyses of a-CPP: comparison of experimental data to 3 computational models

In order to extract the Pair Distribution Function (PDF), X-Ray Diffraction (XRD) measurements were performed with a Bruker D8 ADVANCE diffractometer equipped with a LYNXEYE detector, with Mo Kα radiation (mean $\lambda(K_{\alpha 1 \alpha 2})$ = 0.71073Å) and a Zirconium filter, using the reflection mode. The final XRD pattern (Q_{min} = 1.08 $Å^{-1}$ and Q_{max} = 17 $Å^{-1}$) was obtained from the combination of 3 patterns measured with fixed divergence slit (0.3°) converted in counts per second with the following parameters $2\theta_i$(°)-$2\theta_f$(°)-step size(°)-step time(s): 7-50-0.05-25, 50-90-0.05-50 and 90-148-0.05-100.

The PDFgetX3 program[9] was used for the extraction of the PDF from the experimental XRD pattern (Figure S3), with the rpoly (limitation of the maximum frequency in the F(Q) correction polynomial) and Q_{max} (Q cutoff for the meaningful input intensities) parameters set to 1.63 and 16.6 respectively. PDF curves were also calculated from the 3 computational models using PDFGUI software[10]. Thermal displacements were fixed (U_{ii}=0.005$Å^2$). The particle size was here set at 15 Å in order to mimic the missing long range order of amorphous materials[11].

The experimental and calculated curves were then compared allowing the scale factor to vary for the best fit.

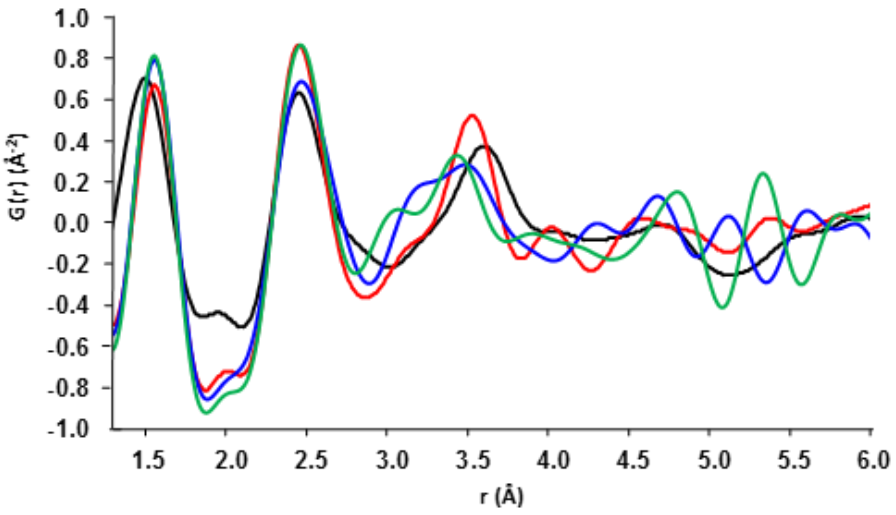

Figure S3. Experimental (black) and calculated (red for model I, blue for model II, green for model III) of the amorphous-$Ca_2P_2O_7.xH_2O$ phase (a-CPP, x ~ 4).

DFT calculation of the NMR parameters using the GIPAW approach

Computational NMR spectra were performed utilizing DFT electronic structure calculations based on the GIPAW method[12] and implemented in the Quantum Espresso code.[13] Norm-conserving pseudopotentials[14] in the Kleinman-Bylander form[15] with generalized gradient approximation (GGA) in the form of Perdew, Burke, and Ernzerhof (PBE)[16] was implemented. An energy cut-off of 80 Ry was used with a 1x1x1 k-point matrix based on the amorphous nature of the system. The initial structural models developed using the AIMD/DFT protocol described above were used as initial inputs and were re-optimized under described electronic structure conditions. Absolute shielding tensors for the computational systems were calculated from fully converged all-electron calculations. To set the ^{43}Ca chemical shift scale, as previously described, the calculated δ_{iso} for a series of reference compounds were compared to experimental values so that the average sum of experimental and calculated shifts coincide.[17] The principal components V_{xx}, V_{yy}, and V_{zz} of the electric field gradient (EFG) tensor were obtained by diagonalization of the traceless EFG tensor. The quadrupolar interaction can then be characterized by the quadrupolar coupling constant C_Q and the asymmetry parameter η_Q, which are defined as: $C_Q = eQV_{zz}/h$ and $\eta_Q = (V_{yy}-V_{xx})/V_{zz}$. The experimental value of the quadrupole moment of ^{43}Ca ($Q = -4.44 \times 10^{-30}$ m^2) was used to calculate C_Q.[18]

Table S3: GIPAW computed ^{43}Ca NMR parameters for the three models (including averages of $C_Q(^{43}Ca)$ and $\delta_{iso}(^{43}Ca)$.

	Model I			Model II			Model III		
	δ_{iso} (ppm)	**C_Q (MHz)**	**η_Q**	**δ_{iso} (ppm)**	**C_Q (MHz)**	**η_Q**	**δ_{iso} (ppm)**	**C_Q (MHz)**	**η_Q**
Ca1	-16.1	-3.84	0.85	-5.5	1.18	0.42	26.9	3.58	0.49
Ca2	46.7	-3.73	0.83	17.7	-2.27	0.51	42.0	4.64	0.60
Ca3	16.9	-3.50	0.46	38.8	-3.37	0.27	64.3	2.16	0.90
Ca4	28.5	2.15	0.92	24.5	4.86	0.30	28.3	-5.70	0.61
Ca5	14.1	-2.52	0.40	5.4	3.45	0.69	-14.1	-2.16	0.71
Ca6	13.5	-5.13	0.30	40.1	-2.05	0.76	-6.9	-2.78	0.63
Ca7	-7.4	-1.55	0.54	27.9	-5.53	0.58	62.3	2.84	0.26
Ca8	24.2	-3.49	0.59	46.7	-2.13	0.88	0.4	4.73	0.99
Ca9	60.6	-1.52	0.85	10.5	-3.82	0.40	15.7	-2.73	0.43
Ca10	12.2	4.60	0.82	19.8	2.36	0.75	9.3	4.24	0.52
Ca11	33.1	-6.54	0.88	43.6	3.76	0.47	28.6	2.66	0.83
Ca12	28.0	-3.67	0.70	1.9	-4.56	0.94	-6.1	3.18	0.95
Average values for the 3 models:			$^{calc,\,avg}\delta_{iso}$ 21.6 ppm			$^{calc,\,avg}\lvert C_Q\rvert$ 3.42 MHz			$^{calc,\,avg}\eta_Q$ 0.64

Structural analysis of Ca local environments in the a-CPP models

Table S4: Analysis of the average Ca…O bond distance, coordination number, and number of coordinated water ligands in 3 models of the amorphous $Ca_2P_2O_7.xH_2O$ phase (a-CPP, x ~ 4). Two different cut-off distances were chosen to describe the Ca coordination environment (2.7 and 3.0 Å).

	Model I					Model II					Model III				
	Coordination number		Average Ca…O distance		n H_2O	Coordination number		Average Ca…O distance		n H_2O	Coordination number		Average Ca…O distance		n H_2O
Cutoff	**2.7 Å**	**3.0 Å**	**2.7 Å**	**3.0 Å**	**2.7 Å**	**2.7 Å**	**3.0 Å**	**2.7 Å**	**3.0 Å**	**2.7 Å**	**2.7 Å**	**3.0 Å**	**2.7 Å**	**3.0 Å**	**2.7 Å**
Ca1	7	7	2.49	2.49	1	7	8	2.51	2.54	0	5	6	2.43	2.49	1
Ca2	6	6	2.35	2.35	3	6	6	2.40	2.40	2	5	5	2.29	2.29	2
Ca3	6	6	2.37	2.37	1	7	7	2.41	2.41	2	5	5	2.39	2.39	2
Ca4	6	6	2.40	2.40	2	5	6	2.36	2.43	1	5	6	2.37	2.45	2
Ca5	7	7	2.40	2.40	2	6	8	2.51	2.57	2	9	9	2.54	2.54	3
Ca6	6	6	2.43	2.43	3	6	6	2.37	2.37	4	7	7	2.45	2.45	4
Ca7	8	8	2.51	2.51	5	5	5	2.35	2.35	1	4	4	2.32	2.32	1
Ca8	7	7	2.46	2.46	4	6	7	2.36	2.42	4	6	8	2.43	2.56	2
Ca9	6	6	2.33	2.33	1	6	8	2.45	2.53	2	6	6	2.38	2.38	2
Ca10	6	6	2.45	2.45	2	6	7	2.41	2.49	2	6	6	2.41	2.41	3
Ca11	6	6	2.36	2.36	1	6	6	2.38	2.38	3	7	8	2.40	2.47	3
Ca12	6	6	2.36	2.36	0	5	5	2.37	2.37	0	6	7	2.43	2.48	1

Simulations using Czjzek (Gaussian Isotropic Model, GIM) and Gaussian isotropic chemical shift distributions.[19]

For both magnetic fields (20.0 and 35.2 T), the initial values of $C_Q(^{43}Ca)$, $\eta_Q(^{43}Ca)$ and $\delta_{iso}(^{43}Ca)$ were obtained by GIPAW calculations (12 Ca sites *per* AIMD model) (see Figure 3a/ in the main text). Following ref. 19, the GIM (Gaussian Isotropic Model) case of the Czjzek distribution was then used for each *individual* calcium site. GIM corresponds to a statistical distribution of charges around the observed nucleus. Such an assumption is *a priori* valid for ^{43}Ca. In Figure S4, various levels of Gaussian isotropic chemical shift distribution were added (from 0 ppm, *i.e.* GIM model, to 20 ppm).

§§§§§FIGURE S4 §§!

Figure S4. Czjzek and Gaussian isotropic chemical shift distributions for a-CPP at 20.0 and 35.2 T.

References

[1] Gras, P.; Rey, C.; Marsan, O.; Sarda, S.; Combes, C. *Eur. J. Inorg. Chem.* **2013**, 5886.
[2] Colas, H.; Bonhomme-Coury, L.; Coelho Diogo, C.; Tielens, F.; Babonneau, F.; Gervais, C.; Bazin, D.; Laurencin, D.; Smith, M. E.; Hanna, J. V.; Daudon, M.; Bonhomme, C. *CrystEngComm,* **2013**, *15*, 8840.
[3] Gervais, C.; Laurencin, D.; Wong, A.; Pourpoint, F.; Labram, J.; Woodward, B.; Howes, A. P.; Pike, K. J.; Dupree, R.; Mauri, F.; Bonhomme, C.; Smith, M. E. *Chem. Phys. Lett*. **2008**, *464*, 42.
[4] Brinkmann, A.; Kentgens, A.P.M. *J. Phys. Chem. B* **2006**, 110, 16089.

[5] Gan, Z.; Kwak, H.-T. *J. Magn. Reson.* **2004**, *168*, 346.
[6] O'Dell, L. A. *Solid State NMR*, **2013**, *55-56*, 28.
[7] Gras, P.; Baker, A.; Combes, C.; Rey, C.; Sarda, S.; Wright, A. J.; Smith, M. E.; Hanna, J. V.; Gervais, C.; Laurencin, D.; Bonhomme, C. *Acta Biomater.* **2016**, *31*, 348.
[8] Tucker, M.G., Keen, D.A., Dove, M.T., Goodwin, A.L., Hui, Q, *J. Phys. Condens. Matter* **2007,** *19,* 335218
[9] Juhás, P.; Davis, T.; Farrow, C. L.; Billinge, S. J. L. *J. Appl. Cryst.* **2013**, *46*, 560.
[10] Farrow, C. L.; Juhas, P.; Liu, J. W.; Bryndin, D.; Boin, E. S.; Bloch, J.; Proffen, T.; Billinge, S. J. L. *J. Phys. Condens. Matter* **2007**, *19*, 335219
[11] T. Proffen, K. L. Page, S. E. McLain, B. Clausen, T. W. Darling, J. A. TenCate, S.-Y. Lee and E. Ustundag, *Zeitschrift für Krist. - Cryst. Mater.*, 2005, **220**, 1002–1008.
[12] Pickard, C. J.; Mauri, F. *Phys. Rev. B* **2001,** *63*, 245101.
[13] Giannozzi, P. B., S.; Bonini, Nicola; Calandra, M.; Car, R.; Cavazzoni, C.; Ceresoli, D.; Chiarotti, G. L.; Cococcioni, M.; Dabo, I.; Dal Corso, A.; Fabris, S.; Fratesi, G.; de Gironcoli, S.; Gebauer, R.; Gerstmann, U.; Gougoussis, C.; Kokalj, A.; Lazzeri, M.; Martin-Samos, L.; Marzari, N.; Mauri, F.; Mazzarello, R.; Paolini, S.; Pasquarello, A.; Paulatto, L.; Sbraccia, C. *J. Phys. Condens. Matter* **2009,** *21*, 395502-1-19.
[14] Troullier, N.; Martins, J. L. *Phys. Rev. B* **1991**, *43*, 1993.
[15] Kleinman, L.; Bylander, D. *Phys. Rev. Lett.* **1982**, *48*, 1425.
[16] Perdew, J. P.; Burke, K.; Ernzerhof, M. *Phys. Rev. Lett.* **1997**, *78*, 1396.
[17] Gervais C., Jones C., Bonhomme C., Laurencin D. *Acta Cryst.* **2017**, *C73*, 208.
[18] Pyykkö, P. *Mol. Phys.* **2008,** *106*, 1965.

[19] Neuville, D.R. ; Cormier L. ; Massiot D. *Geochim. Cosmochim. Acta* **2004**, 68, 5071.